imental Investigation of Micro Heat Pipes Fabricated in Silicon Wafers," *Journal of Heat Transfer*, Vol. 115, 1993, pp. 751–756.

[8]Ha, J. M., and Peterson, G. P., "Analytical Prediction of the Axial Dryout of an Evaporating Liquid Film in Triangular Microgrooves," *Heat Transfer on the Microscale*, American Society of Mechanical Engineers HTD-Vol. 253, 1993, pp. 53–62.

High-Temperature Performance of an Integral Cesium Reservoir in a Thermionic Converter

K. L. Thayer* and M. L. Ramalingam†
UES, Inc., Dayton, Ohio 45432
and
Timothy J. Young‡
Wright Laboratory,
Wright-Patterson Air Force Base, Ohio 45433

Introduction

THE inclusion of cesium reservoirs in thermionic converters has played a vital role in the production of converters that achieve optimum performance.[1] Cesium vapor in the interelectrode space of a thermionic converter reduces the negative space charge effect on the emitter surface and the work functions of the electrodes due to the adsorption of cesium atoms on their surfaces.[2] The dependence of the cesium vapor pressure p_{cs} on the liquid reservoir temperature T_r is given empirically as[1]

$$p_{cs} = [(2.45 \times 10^8)/\sqrt{T_r}]\exp(-8910/T_r), \text{ Torr} \quad (1)$$

for T_r in Kelvin. Because of the exponential dependence of the cesium pressure on the liquid reservoir temperature, a high degree of temperature control is necessary for the reservoir to maintain a constant cesium pressure. As the liquid reservoir temperature typically ranges from 525 to 625 K (≈0.5 to 6 Torr), and the minimum temperature in the core of the thermionic fuel element (TFE) of the advanced thermionic initiative (ATI) reactor design is approximately 880 K, the liquid reservoir would have to be located external to the core, complicating the overall design of the power system with intricate plumbing and valve arrangements.[3]

Due to the problems cited above, integral, solid sorption reservoirs have been evaluated as an alternative to liquid reservoirs for use in the ATI-TFE design. The potential advantages of such a reservoir are as follows:

1) The reservoir could be designed to operate at a temperature intermediate to the emitter and collector temperatures, thus eliminating the electronic hardware associated with liquid reservoir heaters and temperature controllers.

2) Plumbing and other problems associated with the use of liquid cesium could be eliminated.

3) Optimum cesium pressure could be maintained over a wide range of emitter temperatures due to direct temperature feedback from the converter. Harbaugh and Basiulis[4] investigated the storage characteristics of molybdenum and tungsten reservoirs and tested the performance of these reservoirs in actual converters. They demonstrated optimum converter performance with the reservoirs above 973 K, and also found that the cesium pressure in an adsorption reservoir is less sensitive to changes in reservoir temperature than the cesium pressure in a liquid reservoir. The metal reservoirs were ultimately found to be impractical because of their limited storage capabilities and the variation of vapor pressure, at constant temperature, due to loss of cesium.

Other investigators identified graphite as a potential sorption medium. The intercalation of cesium in graphite forms compounds ranging from C_8Cs to $C_{60}Cs$. Salzano and Aronson[5] characterized these compounds and measured the effect of the graphite reservoir temperature on the cesium vapor pressure. The compounds were found to supply cesium vapor at pressures of 0.5–10 Torr via two-phase equilibrium reactions at temperatures ranging from 700 to 1200 K. The cesium pressure was determined to depend only on the graphite temperature and the reservoir compound. Yates[6] analytically determined the response of a single thermionic cell with an integral reservoir to changes in power input and load resistance and found that sorption reservoirs made from the graphite lamellar compounds provided the best overall response to changes in converter operating conditions.

Thermophysical Characteristics of the Cesium Reservoir

Variation of cesium vapor pressure with reservoir temperature for both liquid and graphite reservoirs suggest, for the reservoirs investigated, that the only applicable cesium-graphite reservoir for direct conductive coupling, without an insulation layer, is the $3C_{24}Cs \rightarrow 2C_{36}Cs + Cs(g)$ equilibrium reaction.[7] The experimental data for the cesium pressure from this graphite reservoir was curve-fitted to generate information for the relationship between pressure and temperature of the graphite reservoir. Once the temperature distribution of the emitter lead region was obtained, the temperature limits of the cesium-graphite equilibrium reaction defined the extreme positions for placement of the graphite reservoir in the lead region. The reservoir could be positioned from 17 to 22 mm from the emitter-lead interface as shown in the schematic in Fig. 1.[3]

Analytical Procedure and Lead Region Thermal Analysis

The nonfueled lead region has approximately 25 mm of emitter substrate to allow a direct conduction path for heat transfer from the hot, fueled region to the cesium-graphite metal-matrix reservoir. The thermionic fuel element pin located at the center of the reactor core receives the maximum thermal input power at steady-state operation and is designated the peak power pin. The average power pin is located between the center of the core and the outer surface.

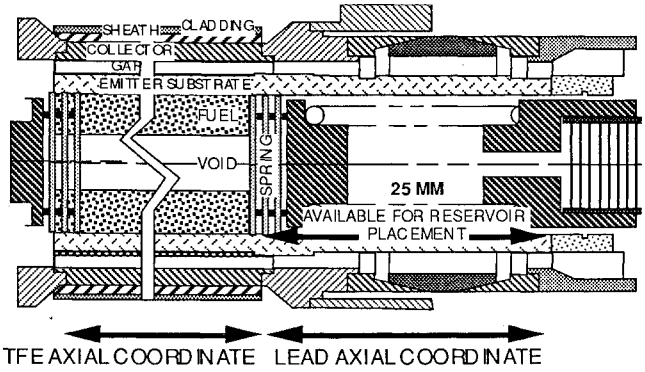

Fig. 1 Schematic of the ATI-TFE design for the location of the reservoir.

Received April 25, 1994; revision received Aug. 25, 1994; accepted for publication Aug. 29, 1994.

*Research Scientist.

†Research Scientist. Associate Fellow AIAA.

‡Engineer, Aerospace Power Division.

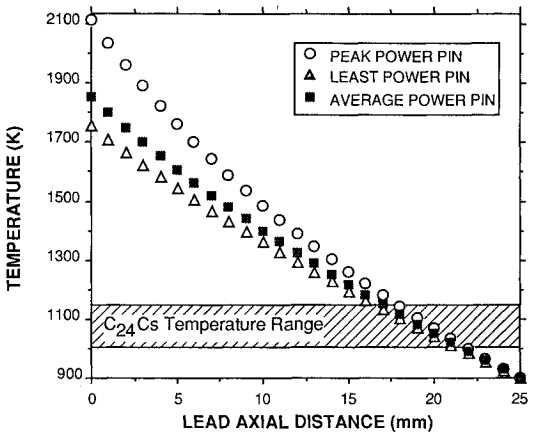

Fig. 2 Calculated temperature distributions in the lead region of the ATI-TFE for three fuel pins.

The cesium vapor pressure from the intercalated cesium-graphite reservoir is dependent upon the temperature of the reservoir matrix. The $3C_{24}Cs \rightarrow 2C_{36}Cs + Cs(g)$ equilibrium reaction is only valid within the temperature range of 1000–1150 K. The placement of a metal matrix cesium reservoir within the ATI single-cell TFE will require determination of the temperature distribution in the lead region. The required cesium pressure for optimum thermionic performance specifies a reservoir location within the lead region. The temperature field shown in Fig. 2 within the lead region was found from an energy balance on a ring-shaped, differential control volume, and included heat conduction, radiation, and generation. Also indicated in the same figure is the region of interest for placing the graphite reservoir for the $C_{24}Cs$ thermodynamic equilibrium reaction.

Results and Conclusions on Thermionic Performance

The simulated electrical converter output characteristics were generated using the CYLCON semi-two-dimensional cylindrical converter thermionic performance model.[3] Input parameters for this set of programs include the emitter o.d., the emitter and collector clad thickness, number of mesh points, the axial distributions of emitter and collector temperature, liquid cesium reservoir temperature, emitter bare work function, TFE length, and current at the ends of the cell. The outputs of the program that include axial distributions for the interelectrode voltage and power densities were then computed for the different graphite reservoir locations (and corresponding cesium pressures). The optimum position for each graphite reservoir was determined by reviewing these distributions. Information and data obtained from the details on the reactor core elements such as the optimum cesium pressure for each pin and its variation with maximum emitter temperature were incorporated in the determination of the axial distributions of interelectrode voltage and power density for the average power pin.

Output Voltage and Power Characteristics

Figure 3 shows the calculated interelectrode voltage distributions for the TFE, vs axial position, for the average power pin. The variation in cesium pressure results from varying the location of the cesium-graphite reservoir in the lead region between the limiting extremes. The interelectrode voltage is strongly dependent upon the cesium pressure and emitter temperature distribution. The voltage increases as the emitter temperature increases, and this can be attributed to the increase in emitter work function ϕ_E with increased emitter temperature in the center of the TFE.[1] As ϕ_E increases, the interelectrode voltage $V \propto \phi_E - \phi_C$ also increases. The axial voltage distribution varies approximately 0.5 V over the pressure range investigated. The optimum cesium pressure for the

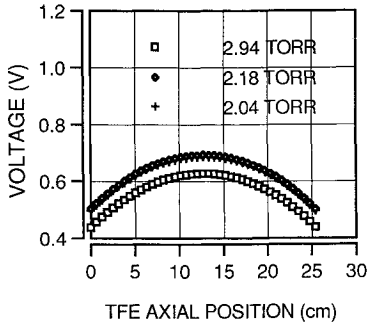

Fig. 3 Axial distribution of interelectrode voltage for various cesium pressures.

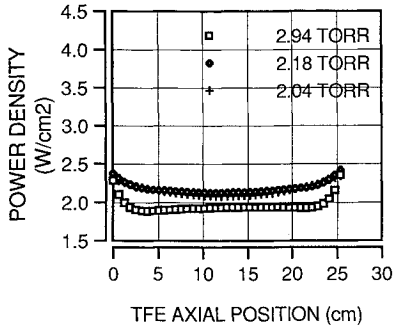

Fig. 4 Axial distributions of output power for various cesium pressures.

average power pin was found to be 2.18 Torr. The different temperature distributions within the TFEs require different cesium pressures for optimum output. The power density distribution calculated by the model for the same TFE is shown in Fig. 4. As described above, the voltage distribution is more dependent upon the cesium pressure than is the current density, and the power density being the product of voltage and current density, is more sensitive to the voltage. In conclusion, the effects on ATI-TFE performance with the inclusion of a cesium-graphite sorption reservoir in the lead region was simulated using a semi-two-dimensional computer model, and the optimum cesium pressures and reservoir locations determined for all the pins in the reactor.

Acknowledgments

Research activities were conducted at the Thermionic facilities of the Wright Laboratory, WPAFB, through UES, Inc., Contract F33615-92-C-2284, sponsored by BMDO/IST. The authors would like to thank Kevin Horner-Richardson of Thermacore, Inc., Lancaster, Pennsylvania, John McVey of Rasor Associates, Inc., Sunnyvale, California, and Andrew Klein of Oregon State University, Corvallis, Oregon, for their assistance.

References

[1]Hatsopoulos, G. N., and Gyftopoulos, E. P., "Thermionic Energy Conversion," *Processes and Devices*, 1st ed., Vol. I, The MIT Press, Cambridge, MA, 1973.

[2]Rasor, N. S., and Warner, C., "Correlation of Emission Processes for Adsorbed Alkali Films on Metal Surfaces," *Journal of Applied Physics*, Vol. 35, No. 9, 1964, pp. 2589–2600.

[3]Ramalingam, M. L., "Advanced Thermionic Technology Initiative Program," U.S. Air Force Wright Lab., WL-TR-91-2082, Dayton, OH, 1991.

[4]Harbaugh, W. E., and Basiulis, A., "The Development of a High-Temperature Reservoir for Automatic Control of Cesium Pressure," *Thermionic Conversion Specialists Conference* (Houston, TX), IEEE, New York, 1966, pp. 243–248.

[5]Salzano, F. J., and Aronson, S., "Thermodynamic Properties of the Cesium-Graphite Lamellar Compounds," *Journal of Chemical Physics*, Vol. 43, No. 1, 1965, pp. 149–154.

[6]Yates, M. K., "Temperature Control and Thermal Coupling of an Integral Adsorption-Type Cesium Reservoir," *Thermionic Conversion Specialists Conference* (Houston, TX), IEEE, New York, 1966, pp. 249–258.

[7]Horner-Richardson, K. D., and Kim, K. Y., "Sorption Reservoirs for Thermionic Converters," *Ninth Symposium on Space Nuclear Power Systems* (Albuquerque, NM), American Inst. of Physics, New York, 1992, pp. 629–637.

Transient Conductive and Radiative Heat Transfer in a Silica Window

Ming-Horng Su* and William H. Sutton†
University of Oklahoma, Norman, Oklahoma 73019

Nomenclature

h	=	convective heat transfer coefficient
I	=	intensity, I^+, I^- denote positive and negative η directions, respectively
$I_{\lambda b}$	=	Planck's distribution function
L	=	thickness
n	=	refractive index
Q^c	=	dimensionless conduction heat flux, $q_i^c/h(T_{aw} - T_{\infty 1})$
Q^r	=	dimensionless net radiation heat flux, $q_i^r/h(T_{aw} - T_{\infty 1})$
q^r	=	net radiative heat flux
q_i^r	=	net radiative heat flux at node i
T	=	temperature
T_{aw}	=	adiabatic wall temperature
T_0	=	initial temperature
$T_{\infty 1}$, $T_{\infty 2}$	=	ambient temperature at the first and second boundary
t	=	time
z	=	position
α	=	thermal diffusivity, $k/\rho^* c_p$, thermal conductivity/(density × specific heat)
Δ	=	increment
η	=	dimensionless axial coordinate, z/L
Θ	=	dimensionless temperature, $T/T_{\infty 1}$
θ_{cr}	=	critical angle
θ_2	=	refracted internal polar angle
κ	=	absorption coefficient
λ	=	wavelength
ρ^*	=	density
ρ_i, ρ_o	=	reflectivity inside and outside of glass

Subscript

λ	=	wavelength dependency

Introduction

THE purpose of this study is to present solutions for the transient temperature distribution in a nongray electromagnetic window, externally heated by time-independent convective flux for high-speed flow, for a short time interval (5 s). The temperature variation within the window is important because its electromagnetic transmission characteristics are dependent upon temperature. The window is modeled as a one-dimensional slab with directional-dependent specularly reflecting surfaces described by the Fresnel relations. The convective heat transfer coefficient is specified. Several investigators have analyzed combined conductive and radiative heat transfer in a one-dimensional medium,[1,2] but with different boundary conditions or conditions than those used there.

Formulation

The governing differential transient energy equation for temperature is

$$\rho^* c_p \frac{\partial T}{\partial t} + \frac{\partial}{\partial z}\left[-k\frac{\partial T}{\partial z} + q^r\right] = 0 \qquad 0 < z < L, \quad t > 0 \tag{1}$$

The boundary conditions are

$$[h(T_{aw} - T) + q^r]_{z=0^-} = \left[-k\frac{\partial T}{\partial z} + q^r\right]_{z=0^+}, \qquad t > 0 \tag{2}$$

$$\left[-k\frac{\partial T}{\partial z} + q^r\right]_{z=L^-} = [q^r]_{z=L^+}, \qquad t > 0 \tag{3}$$

where q^r is evaluated, as noted, independently on each side of the boundary interface. The values are expected to be equal in the analytical sense, but could vary in the finite difference model. The initial condition is

$$T(z, 0) = T_0, \qquad 0 \le z \le L \tag{4}$$

The radiative transfer equation for a nongray, absorbing and emitting slab is

$$\cos\theta_2 \frac{\partial I_\lambda}{\partial z} + \kappa_\lambda I_\lambda = \kappa_\lambda I_{b\lambda}[T(z)] \qquad 0 < z < L, \quad 0 < \theta_2 < \frac{\pi}{2} \tag{5}$$

The radiative boundary conditions with specular Fresnel reflection are

$$I_\lambda^+(0, \theta_2) = (1 - \rho_o) I_{\lambda b}[T_{\infty 1}] + \rho_i I_\lambda^-(0, \theta_2) \qquad 0 < \theta_2 < \theta_{cr} \tag{6}$$

$$I_\lambda^+(0, \theta_2) = I_\lambda^-(0, \theta_2), \qquad \theta_{cr} < \theta_2 < \pi/2 \tag{7}$$

$$I_\lambda^-(L, \theta_2) = (1 - \rho_o) I_{\lambda b}[T_{\infty 2}] + \rho_i I_\lambda^+(L, \theta_2) \qquad 0 < \theta_2 < \theta_{cr} \tag{8}$$

$$I_\lambda^-(L, \theta_2) = I_\lambda^+(L, \theta_2), \qquad \theta_{cr} < \theta_2 < \pi/2 \tag{9}$$

When a beam is incident on the interface from the glass side, ρ_i may be calculated by substituting $1/n$ for n, for all θ_2 less than θ_{cr}; above this angle, the beams undergo total internal reflection and $\rho_i = 1$ so that the reflectivity from the glass side ρ_i and the reflectivity from the air side ρ_o are considerably different.

The external hemispherical solid angle is remapped through Snell's law into a smaller cone of radiation with angle θ_2 depending on nongray refractive indexes; therefore, the in-

Received Feb. 19, 1993; revision received Feb. 28, 1994; accepted for publication Feb. 28, 1994.

*Research Associate, School of Aerospace and Mechanical Engineering.

†Associate Professor, School of Aerospace and Mechanical Engineering.